THE JOURNAL OF PHYSICAL CHEMISTRY C

ARTICLE

pubs.acs.org/JPCC

Band Lineup and Charge Carrier Separation in Mixed Rutile-Anatase Systems

Peter Deák,* Bálint Aradi, and Thomas Frauenheim

Bremen Center for Computational Materials Science, University of Bremen, PoB 330440, D-28334 Bremen, Germany

ABSTRACT: Calculations by the HSE06 functional for rutile and anatase crystals reproduce the observed width of the valence and conduction bands, as well as of the gap. From the band structures the branching point energies are obtained as reference for both phases, allowing us to deduce a generic band alignment scheme without a specific interface model. The results show that both bands of rutile lie higher than those of anatase, so in mixed systems the holes are accumulated in the former while the electrons in the latter. Consequences for photocatalytic and photoelectrochemical applications are discussed.

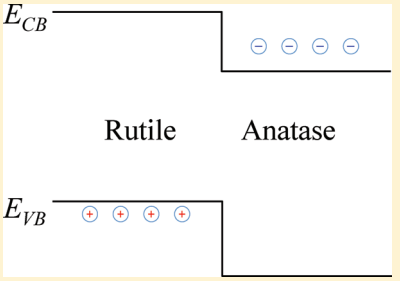

Since Fujishima and Honda discovered the photocatalytic splitting of water on a TiO_2 electrode under ultraviolet light,[1] the enormous amount of research invested in TiO_2 has led to many promising applications in "energy" and "environment" related areas, ranging from photovoltaics and photocatalysis to photo/electrochromics and sensors. An intriguing and often encountered phenomenon in TiO_2 photochemistry is that mixed phases of anatase and rutile exhibit higher activity than their pristine compositions.[2−6] Although not yet fully understood,[7] the effect is believed to involve photoexcited charge migration between the two phases, which in turn enhances charge separation.[5,8,9] The migration across the anatase/rutile interface is supposed to be the result of a staggered band alignment. This hypothesis has been difficult to test, however, due to the lack of model TiO_2 systems with well-defined anatase/rutile interfaces that are amenable to experimental techniques. Work function measurements by photoelectron spectroscopy (PES),[10] as well as determination of the flat band potential with a standard electrode,[11] in rutile and anatase separately (on specific surfaces), found that the Fermi level in rutile lies 0.2 eV higher than in anatase. PES measurement (on the same surfaces) of the Fermi-level position[10] found it very close to the conduction band (CB) in both crystals, indicating that the work function difference corresponds to an offset of the CBs. The same conclusion was reached in ref 11 as well. However, since the work function can strongly vary with surface orientation and preparation, this scheme is not generally accepted, and both alignment between the conduction bands[12] and between the valence bands (VB)[13] has been postulated.

A theoretical method which requires no knowledge of the structural details of the interface for calculating band lineups is based on the branching point energy (BPE) or charge neutrality level[14−16] as common reference. The BPE can be computed as the average of midgap energies.[14,15,17−19] Recently, this method has been applied successfully to compute band lineups between III-nitrides and III-/II-oxides[20] and between silicon and various transparent conducting oxides,[21] based on band structures obtained by the GW method. In the present paper we show that in the particular case of rutile and anatase TiO_2, the HSE06 functional reproduces the GW electronic structure. So we use the HSE06 results to determine the BPE and the band lineup. We find that the CB of rutile lies higher in energy than that of anatase by about 0.3−0.4 eV. This finding explains the enhanced charge separation in mixed systems, as origin of the observed high photocatalytic activity.

Electronic structure calculations have been carried out using the HSE06 screened hybrid exchange functional[22,23] in the Vienna ab initio simulation package, VASP 5.2.8, with the projector augmented wave (PAW) method.[24] The $3s^2$ shell was included in the core of Ti. The electronic structures for rutile and anatase have been calculated in the respective primitive cells with a 8 × 8 × 8 Monkhorst−Pack (MP) set,[25] reduced by a factor of 2 in the Fock-exchange part.[26] Convergence of the total energy has been achieved by setting the plane-wave cutoff for the wave function expansion (and for that of the charge density) to 420 (840) eV. The geometry was found by minimizing the total energy until the forces fell below 0.02 eV/Å. The BPE was calculated as the weighted average of midgap energies over the MP set:[20]

$$E_{\mathrm{BP}} = \frac{1}{2N_k}\sum_k \left[\frac{1}{N_{\mathrm{CB}}}\sum_i^{N_{\mathrm{CB}}} \varepsilon_{C_i} + \frac{1}{N_{\mathrm{VB}}}\sum_i^{N_{\mathrm{VB}}} \varepsilon_{V_i}\right] \qquad (1)$$

where $N_{\mathbf{k}}$ is the number of points in the $\mathbf{k}$ mesh, N_{CB} and N_{VB} are the number of conduction and valence bands, ε_{C_i} and ε_{V_i}, respectively, taken into account in determining the midgap value.

The equilibrium lattice constants (in comparison to experiment)[27] were found to be a = 4.567 Å (4.587 Å), c = 2.944 Å (2.954 Å), and u = 0.305 (0.305) for rutile, and 3.755 Å (3.782 Å), c = 9.561 Å (9.502 Å), and u = 0.207 (0.208) for anatase. The agreement with experiment is better than the one obtained by the local density approximation (LDA).[28] The calculated direct band gap of rutile,

Received: December 4, 2010
Revised: January 7, 2011
Published: February 04, 2011

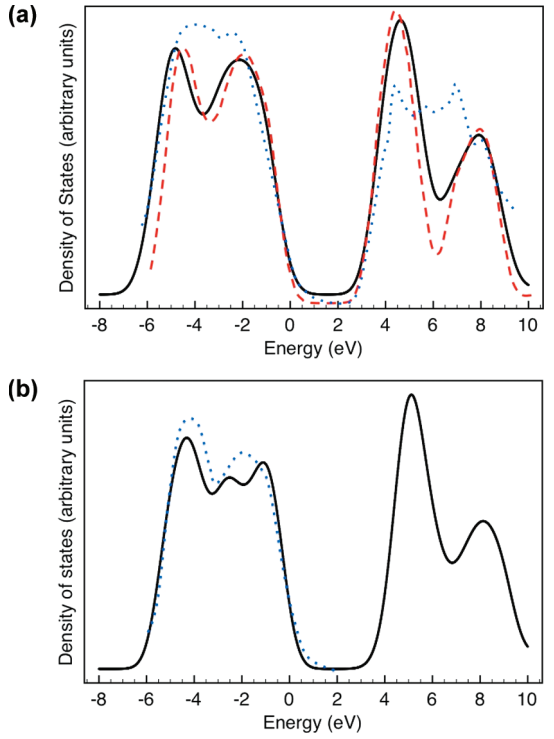

Figure 1. DOS of rutile (a) and anatase (b) from the present HSE06 calculation (solid lines), compared to the experimentally observed PES and IPES for rutile[30] and PES for anatase[39] (dotted lines). Also shown is the DOS for rutile from the GW calculation of ref 29 (dashed line). Both DOS curves were calculated with a Gaussian broadening of $\sigma = 0.5$ eV. The spectra were aligned by the slope of the VB edge.

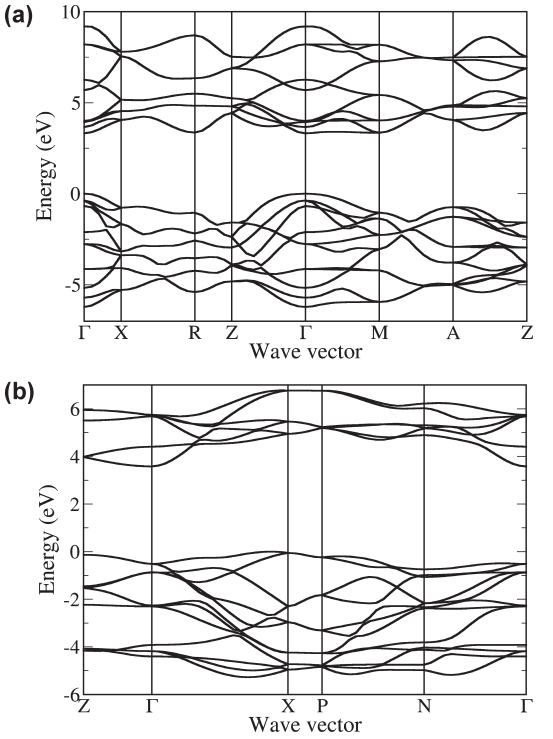

Figure 2. HSE06 band structure of rutile (a) and anatase (b).

Table 1. Branching Point Energy (BPE) with Respect to the VB Edge, Calculated by Different Choices of N_{VB} and N_{CB}

		BPE		rutile−anatase	
N_{VB}	N_{CB}	rutile	anatase	ΔE_{CB}	ΔE_{VB}
1	1	1.48	2.06	0.38	0.59
2	1	1.38	2.00	0.41	0.62
2	2	1.47	2.06	0.38	0.59
4	4	1.43	1.98	0.34	0.55
12	10	1.33	1.83	0.29	0.50

3.37 eV, and the indirect ($0.85\Delta \rightarrow \Gamma$) band gap of anatase, 3.58 eV, are in excellent agreement with the results of a recent full frequency dependent G_0W_0 calculation,[29] 3.34 and 3.56 eV, respectively. In the case of rutile, the band gap deduced from PES and inverse photoelectron (IPES) spectroscopy,[30] 3.3 eV, confirm these results. Note that the low temperature optical band gap for rutile and anatase was measured to be 3.04 and 3.42 eV, respectively.[31,32] The higher values of all GW calculations[33] are explained by electron−phonon interactions, irrelevant for PES data.[29,33]

Figure 1 compares the HSE06 density of states (DOS) for both modifications to the photoelectron spectra[30] and to the available GW result on rutile.[29] As can be seen, the two DOS, calculated with the same broadening parameter for rutile are very close to each other. The VB is slightly broader in HSE06 and closer to the experimental band widths than in GW. In the case of anatase only PES of the valence band is available, and the agreement of the HSE06 result to that is very good. (We also note that HSE06 in TiO_2 shows the correct linear dependence of the total energy on the fractional occupation numbers[34] and correctly predicts the observed Burnstein−Moss shift in anatase on Nb-doping.[35]) On the basis of these tests, we have used the HSE06 band structure directly to calculate the BPE.

There is a certain amount of uncertainty connected with the choice of N_{VB} and N_{CB} in eq 1.[20] Figure 2 shows the HSE06 band structures of both modifications. (We note that apart form the width of the bands and the gap, the HSE06 results are quite similar to the LDA ones in Figure 1 of ref 28.) The VB of TiO_2 consists of twelve branches dominated by O2p states, while the lower part of the CB is determined by the ten Ti3d states. (N.B. both primitive cells contain two TiO_2 units.) As can be seen, the topmost two branches of the VB (both degenerate at the zone center, Γ) cross each other in both rutile and anatase. The two lowest branches of the CB are nondegenerate in Γ but meet each other and the following branch (which is degenerate in Γ) at the zone boundaries. However, as can be seen from Table 1, the choice of N_{VB} and N_{CB} has little influence on the calculated BPE.

From these results we conclude that the bulk conduction band edge of rutile lies between about 0.3 and 0.4 eV above that of anatase, while the VB offset is 0.5−0.6 eV. This is schematically shown in Figure 3. The CB offset found here is higher than the one that can be deduced from PES for the rutile (100) and anatase (001) surfaces:[10] using our gap values, the measured Fermi-level positions and work functions result in an offset of 0.1 eV (with the CB of rutile being higher). Also the VB offset, deduced for anatase-covered rutile particles,[13] ~0.2 eV is smaller than our value but is in the same direction. We emphasize, however, that our offsets are "generic" values, obtained independently of the interface structure. It was shown that the work function may change by about 0.1 eV from surface to surface,[36] and even more on change of the defect structure.[37] Still our results reinforce the specific data of refs 10, 11, and 13 that

dx.doi.org/10.1021/jp1115492 |J. Phys. Chem. C 2011, 115, 3443–3446

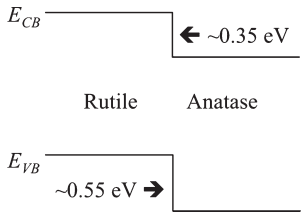

Figure 3. Schematic representation of the band lineup between rutile and anatase.

qualitatively a line-up as in Figure 2 can be expected most of the time, while an alignment of the VBs[12] is less likely.

In summary, by calculating the branching point energy of the HSE06 band structures of rutile and anatase, we have found the band lineup shown schematically in Figure 3. This staggered alignment of the bands means that migrating holes accumulate in rutile, while electrons in anatase. As pointed out earlier, charge separation enhances the photochemical activity of mixed phase TiO_2 powders. The present results show that the separation may be much stronger than considered before and concerns both carrier types. The "staggering" found here in the other direction (rutile being higher than anatase) as postulated before, will steer ideas about possible oxidative or reductive reactions pathways that can thermodynamically take place on rutile and anatase.[38] The design of mixed-phase photocatalytic systems for specific purposes will be profoundly influenced by the knowledge of the site for reactions. This allows us, e.g., to selectively tune the properties of one component by doping or by (precious) catalytic metal coverage, diminishing the costs. In future devices with more structured junctions, the design of current flow direction will also have to take this line-up into account.

AUTHOR INFORMATION

Corresponding Author

*E-mail: deak@bccms.uni-bremen.de.

ACKNOWLEDGMENT

Support of the Supercomputer Center of Northern Germany (HLRN Grant No. hbc00001) is highly appreciated. Discussions with L. Mädler are gratefully acknowledged.

REFERENCES

(1) Fujishima, A.; Honda, K. Electrochemical Photolysis of Water at a Semiconductor Electrode. *Nature* **1972**, *238*, 37–38.

(2) Ohno, T.; Tokieda, K.; Higashida, S.; Matsumura, M. Synergism Between Rutile and Anatase TiO_2 Particles In Photocatalytic Oxidation of Naphthalene. *Appl. Catal., A* **2003**, *244*, 383–391.

(3) Sun, B.; Vorontsov, A. V.; Smirniotis, P. G. Role of Platinum Deposited on TiO_2 in Phenol Photocatalytic Oxidation. *Langmuir* **2003**, *19*, 3151–3156.

(4) Liu, Z.; Zhang, X.; Nishimoto, S.; Jin, M.; Tryk, D. A.; Murakami, T.; Fujishima, A. Anatase TiO_2 Nanoparticles on Rutile TiO_2 Nanorods: A Heterogeneous Nanostructure via Layer-by-Layer Assembly. *Langmuir* **2007**, *23*, 10916–10919.

(5) Li, G.; Ciston, S.; Saponjic, Z. V.; Chen, L.; Dimitrijevic, N. M.; Rajh, T.; Gray, K. A. Synthesizing Mixed-Phase TiO_2 Nanocomposites Using A Hydrothermal Method for Photooxidation and Photoreduction Applications. *J. Catal.* **2008**, *253*, 105–110.

(6) Zachariah, A.; Baiju, K. V.; Deepa, K. S.; James, J.; Warrier, K. G. K. Synergistic Effect in Photocatalysis as Observed for Mixed-Phase Nanocrystalline Titania Processed via Sol-Gel Solvent Mixing and Calcination. *J. Phys. Chem. C* **2008**, *112*, 11345–11356.

(7) Ohtani, B. Preparing Articles on Photocatalysis—Beyond the Illusions, Misconceptions, and Speculation. *Chem. Lett.* **2008**, *37*, 217–229.

(8) Komaguchi, K.; Nakano, H.; Araki, A.; Harima, Y. Photoinduced electron transfer from anatase to rutile in partially reduced TiO_2 (P-25) nanoparticles: An ESR study. *Chem. Phys. Lett.* **2006**, *428*, 338–342.

(9) Di Paola, A.; Bellardita, M.; Ceccato, R.; Palmisano, L.; Parrino, F. Highly Active Photocatalytic TiO_2 Powders Obtained by Thermohydrolysis of $TiCl_4$ in Water. *J. Phys. Chem. C* **2009**, *113*, 15166–15174.

(10) Xiong, G.; Shao, R.; Droubay, T. C.; Joly, A. G.; Beck, K. M.; Chambers, S. A.; Hess, W. P. Photoemission Electron Microscopy of TiO_2 Anatase Films Embedded with Rutile Nanocrystals. *Adv. Funct. Mater.* **2007**, *17*, 2133–2138.

(11) Kavan, L.; Grätzel, M.; Gilbert, S. E.; Klemenz, C.; Scheel, H. J. Electrochemical and Photoelectrochemical Investigation of Single-Crystal Anatase. *J. Am. Chem. Soc.* **1996**, *118*, 6716–6723. Kalyanasundaram, K.; Grätzel, M. Applications of functionalized transition metal complexes in photonic and optoelectronic devices. *Coord. Chem. ReV.* **1998**, *77*, 347–414.

(12) Kho, Y. K.; Iwase, A.; Teoh, W. Y.; Mädler, L.; Kudo, A.; Amal, R. Photocatalytic H_2 Evolution over TiO_2 Nanoparticles. The Synergistic Effect of Anatase and Rutile. *J. Phys. Chem. C* **2010**, *114*, 2821–2829.

(13) Gesenhues, U. Oberflächenaufbau und photochemische Aktivität verschieden stark calcinierter Rutilpigmente. *Farbe + Lack* **1994**, *100*, 244–248.

(14) Tersoff, J. Theory of Semiconductor Heterojunctions: The Role of Quantum Dipoles. *Phys. Rev. B* **1984**, *30*, 4874–4877.

(15) Flores, F.; Tejedor, C. Energy Barriers and Interface States at Heterojunctions. *J. Phys. C* **1979**, *12*, 731–749.

(16) Van de Walle, C. G.; Neugebauer, J. Universal Alignment of Hydrogen Levels in Semiconductors, Insulators and Solutions. *Nature (London)* **2003**, *423*, 626–628.

(17) Tejedor, S.; Flores, F. A Simple Approach to Heterojunctions. *J. Phys. C* **1977**, *11*, L19–L23.

(18) Tersoff, J. Schottky Barriers and Semiconductor Band Structures. *Phys. Rev. B* **1985**, *32*, 6968–6971.

(19) Cardona, M.; Christensen, N. E. Acoustic Deformation Potentials and Heterostructure Band Offsets in Semiconductors. *Phys. Rev. B* **1987**, *35*, 6182–6194.

(20) Schleife, A.; Fuchs, F.; Rödl, C.; Furthmüller, J.; Bechstedt, F. Branch-Point Energies and Band Discontinuities of III-Nitrides and III-/II-Oxides from Quasiparticle Band-Structure Calculations. *Appl. Phys. Lett.* **2009**, *94*, 012104.

(21) Höffling, B.; Schleife, A.; Fuchs, F.; Rödl, C.; Bechstedt, F. Band Lineup between Silicon and Transparent Conducting Oxides. *Appl. Phys. Lett.* **2010**, *97*, 032116.

(22) Heyd, J.; Scuseria, G. E.; Ernzerhof, M. Hybrid Functionals Based on a Screened Coulomb Potential. *J. Chem. Phys.* **2003**, *118*, 8207–8215.

(23) Krukau, A. V.; Vydrov, O. A.; Izmaylov, A. F.; Scuseria, G. E. Influence of the Exchange Screening Parameter on The Performance of Screened Hybrid Functionals. *J. Chem. Phys.* **2006**, *125*, 224106.

(24) Kresse, G.; Hafner, J. Ab Initio Molecular-Dynamics Simulation of the Liquid-Metal−Amorphous-Semiconductor Transition in Germanium. *Phys. Rev. B* **1994**, *49*, 14251–14269. Kresse, G.; Furthmüller, J. Efficient Iterative Schemes for Ab Initio Total-Energy Calculations Using a Plane-Wave Basis Set. *Phys. Rev. B* **1996**, *54*, 11169–11186. Kresse, G.; Joubert, D. From Ultrasoft Pseudopotentials to the Projector Augmented-Wave Method. *Phys. Rev. B* **1999**, *59*, 1758–1775.

(25) Monkhorst, H. J.; Pack, J. K. Special Points for Brillouin-Zone Integrations. *Phys. Rev. B* **1976**, *13*, 5188–5192.

(26) Paier, J.; Marsman, M.; Hummer, K.; Kresse, G.; Gerber, I. C.; Angyan, J. G. Screened Hybrid Density Functionals Applied to Solids. *J. Chem. Phys.* **2006**, *124*, 154709.

(27) Muscat, J.; Swamy, W.; Harrison, N. M. First-Principles Calculations of the Phase Stability of TiO_2. *Phys. Rev. B* **2002**, *65*, 224112and references therein.
(28) Mikami, M.; Nakamura, S.; Kitao, O.; Arakawa, H.; Gonze, X. First-Principles Study of Titanium Dioxide: Rutile and Anatase. *Jpn. J. Appl. Phys.* **2000**, *39*, L847–L850.
(29) Kang, W.; Hybertsen, M. S. Quasiparticle and Optical Properties of Rutile and Anatase TiO_2. *Phys. Rev. B* **2010**, *82*, 085203.
(30) Tezuka, Y.; Shin, S.; Ishii, T.; Ejima, T.; Suzuki, S.; Sato, S. Photoemission and Bremsestrahlung Isochromat Sprectroscopy Studies of TiO_2 (Rutile) and $SrTiO_3$. *J. Phys. Soc. Jpn.* **1994**, *63*, 347–357.
(31) Tang, H.; Lévy, F.; Berger, H.; Schmid, P. E. Urbach Tail of Anatase TiO_2. *Phys. Rev. B* **1995**, *52*, 7771–7774.
(32) Pascual, J.; Camassel, J.; Mathieu, H. Fine Structure in the Intrinsic Absorption Edge of TiO_2. *Phys. Rev. B* **1978**, *18*, 5606–5614.
(33) Chiodo, L.; García-Lastra, J. M.; Iacomino, A.; Ossicini, S.; Zhao, J.; Petek, H.; Rubio, A. Self-Energy and Excitonic Effects in the Electronic and Optical Properties of TiO_2 Crystalline Phases. *Phys. Rev. B* **2010**, *82*, 045207and references therein. Note that GW calculations within the plasmon pole approximation give even higher gap values.
(34) Deák, P.; Aradi, B.; Frauenheim, T. Polaronic Effects in TiO_2 Calculated by the HSE06 Hybrid Functional: Dopant Passivation by Carrier Self-Trapping. Manuscript to be published.
(35) Huy, H. A.; Aradi, B.; Frauenheim, T.; Deák, P. Calculation of the Carrier Concentration Dependent Effective Mass in Nb-Doped Anatase Crystals of TiO_2. Manuscript to be published.
(36) Imanishi, A.; Tsuji, E.; Nakato, Y. Dependence of the Work Function of TiO_2 (Rutile) on Crystal Faces, Studied by a Scanning Auger Microprobe. *J. Phys. Chem. C* **2007**, *111*, 2128–2132.
(37) Schierbaum, K. D.; Fischer, S.; Torquemada, M. C.; de Segovia, J. L.; Román, E.; Martin-Gago, J. A. The Interaction of Pt With TiO_2(110) Surfaces: A Comparative XPS, UPS, ISS, and ESD Study. *Surf. Sci.* **1996**, *345*, 261–273.
(38) Chen, X.; Shen, S.; Guo, L.; Mao, S. S. Semiconductor-based Photocatalytic Hydrogen Generation. *Chem. Rev.* **2010**, *110*, 6503–6570.
(39) Sanjinés, R.; Tang, H.; Berger, H.; Gozzo, F.; Margaritondo, G.; Lévy, F. Electronic Structure of Anatase TiO_2 Oxide. *J. Appl. Phys.* **1994**, *75*, 2945–2951.